Check for updates

Stability study and structural insights into cannabidiol cocrystals†

Adéla Koryťáková, [ID] [a] Argyro Chatziadi, [a] Jan Rohlíček, [b] Eliška Zmeškalová, [ab] Josef Beránek [c] and Miroslav Šoóš [ID] *[a]

Cannabidiol (CBD) is a non-psychoactive compound derived from cannabis and has attracted considerable attention due to its potential therapeutic benefits. It is increasingly used in various health-related products, including dietary supplements, because of its positive effects on pain relief, antioxidative properties, and protection against cell damage. Despite its promising applications, CBD faces significant challenges for oral administration, primarily due to its low solubility, low melting point (67 °C), and poor stability. In this work, we used various methods for CBD cocrystal preparation to improve properties of CBD. We succeeded in preparing five cocrystals, which were fully characterized using several analytical tools, such as X-ray powder diffraction, differential scanning calorimetry, and nuclear magnetic resonance. Notably, the cocrystals increased their melting points compared to pure CBD. Furthermore, the intrinsic dissolution rate was measured for pure CBD and the multicomponent forms to describe the rate of release of CBD from the cocrystal. Finally, the crystal structures of three cocrystals were used to interpret the stability and degradation behaviour of the CBD cocrystals under accelerated conditions. Remarkably, the cocrystals CBD–4,4′-bipyridine and CBD–L-proline remained stable and unaffected for a longer period under stress conditions compared to the pure CBD. This study provides valuable insight into the stability behaviour of the cocrystals under various conditions.

1. Introduction

Phytocannabinoids, which are naturally occurring compounds in the *Cannabis sativa* plant (which is commonly known as hemp), have been used for a long time as a medicine for the treatment of pain, nausea, and insomnia.[1,2] They are a wide group of phytochemicals consisting of approximately 70 compounds, including the well-known psychoactive compound tetrahydrocannabinol (THC), as well as non-psychoactive cannabigerol (CBG), cannabinol (CBN), cannabichromene (CBC) and cannabidiol (CBD). The cannabis plant also contains other natural compounds such as flavonoids, alkaloids, and terpenes, which may influence the biological activity of the plant.[2,3]

CBD has emerged as a promising compound due to its non-psychoactive nature and therapeutic potential. Its mechanism of action, mediated by the endocannabinoid system, plays a crucial role in pain and inflammation modulation[4] and it has been shown to reduce spasticity in animal models.[5] Furthermore, it has additional benefits in treating insomnia, anxiety, depression, autism, rheumatoid arthritis, and neurodegenerative disorders.[5,6] Despite all possible medical benefits, CBD has limited pharmaceutical formulations available. Notable examples of the only formulations approved by the FDA and EMA are Epidiolex[7] (a sesame oil solution) and Sativex,[8] (an alcohol-based spray containing CBD and THC in a 1:1 ratio). However, other strategies to improve CBD bioavailability have been suggested, including self-emulsifying drug delivery systems,[9] intranasal sol–gels[10] and cyclodextrin complexes.[11] The lack of solid dosage forms of CBD represents a significant gap in the market, particularly given their advantages in patient convenience, compliance, dosing precision, and stability.[12,13]

The development of oral solid-state forms for CBD faces considerable challenges. The main limitations are its high lipophilicity (log P 6.3) and low solubility in water (12.6 mg l^{-1}), which lead to poor oral bioavailability.[1,10,14,15] Previous studies have explored strategies like salt formation,[16]

[a] Department of Chemical Engineering, University of Chemistry and Technology in Prague, Technická 3, 16628, Prague 6, Czech Republic. E-mail: miroslav.soos@vscht.cz
[b] Institute of Physics of the Czech Academy of Sciences, Na Slovance 2, 182 00, Prague 8, Czech Republic
[c] Zentiva k.s, U Kabelovny 130, 10237, Prague 10, Czech Republic

amorphous solid dispersion,[17,18] and polymorphism[19] to address these issues, with mixed success. For example, while salts improved the dissolution profiles, they faced significant stability problems, requiring storage at lower temperatures under a nitrogen atmosphere. Furthermore, the new CBD polymorph exhibited a melting point of around 43–46 °C, which is lower than the CBD stable form with a melting point of 67 °C. Finally, amorphous solid dispersions were stable for only 3 months, so they were not suitable for long term stability.[17,18]

Cocrystallization has emerged as a promising strategy to enhance the physicochemical properties of active pharmaceutical ingredients (APIs), including solubility, dissolution rate and stability.[20–22] Cocrystals are crystalline systems, which consist of two or more components in a defined stoichiometric ratio.[20,23] Cocrystals used in the pharmaceutical industry are called pharmaceutical cocrystals and they are multicomponent forms formed from active pharmaceutical ingredients (APIs) and usually inactive and pharmaceutically acceptable compounds (Generally Recognized as Safe, GRAS). The molecules of a cocrystal are bonded by non-bonding interactions, such as hydrogen bonding, van der Waals forces, or π–π interactions. In the case of CBD, there are five cocrystals mentioned in the patent literature,[24,25] namely, CBD–4,4′-bipyridine (BP), CBD–betaine (BE), CBD–L-carnitine (CR), CBD–L-proline (PR) and CBD–tetramethylpyrazine (TMP). However, these cocrystals have not been studied extensively, with the exception of the CBD–TMP cocrystal which is currently undergoing a nonclinical phase of pharmaceutical development known as ART 12.11 targeting treatment of anxiety disorders.[26,27]

Besides the low bioavailability challenges, CBD faces also stability problems particularly under exposure to light, heat and acidic or basic environments,[6,28–30] which is also an important aspect for further pharmaceutical drug development. While stability studies on CBD solutions and oil-based formulations have provided valuable insights, there is limited information on the stability of solid-state CBD and its cocrystals.[6,31–34] Existing studies suggest that the stability of CBD in its solid-state form is more influenced by heat than by humidity.[35]

This study addresses these gaps by focusing on the stability and physicochemical characterization of CBD cocrystals. Our first goal was to perform an extensive cocrystal screening to identify new CBD cocrystals with improved physicochemical properties. From this screening, one new cocrystal was synthesized with piperazine (PI), which has not been previously reported in the patent literature. In addition, we re-synthesised the known cocrystals (CBD–BP, CBD–CR, CBD–PR, CBD–BE, CBD–TMP) with the purpose of investigating more extensively their physicochemical properties and behaviour. The chemical structures of CBD and the corresponding coformers that lead to cocrystal formation are shown in Fig. 1.

To gain a deep insight into their stability and understand better their behaviour, the characterization included their crystal structure determination (for CBD and three cocrystals, where it was possible) and interaction energy calculations. Furthermore, we conducted a dissolution study for the cocrystals and pure CBD using intrinsic dissolution rate measurement to describe their dissolution profile from the cocrystal. In addition, we conducted accelerated stability studies and hygroscopicity measurements to predict the degradation behaviour and assess the potential for long-term storage under practical conditions. They also reduce the costs compared to the classic stability studies, which are usually long-term and recommended by the International Council for Harmonisation.[36] By focusing on the stability and degradation behaviour of CBD cocrystals, this study provides valuable insights into their potential as stable and effective solid forms for pharmaceutical development.

2. Materials and methods

2.1. Materials

Cannabidiol was purchased from PharmaHemp d.o.o. (Ljubljana, Slovenia). The coformers (namely, 2,2′-bipyridine; 4,4′-bipyridine; 4-methylpyridine-N-oxide; L-arginine; caffeine; L-carnitine; L-cysteine; L-glutamic acid; L-glutamine; L-glycine; hippuric acid; indole; isonicotinic acid N-oxide; isonicotinamide; lidocaine; L-lysine; nicotinamide; L-phenylalanine; piperazine; polydatin; L-proline; pyridine-N-oxide; quercetin; riboflavin; tetramethylpyrazine; L-tryptophan; L-tyrosine; L-valine) were purchased from Sigma-Aldrich (St. Louis, USA) and were used as received. All coformers have purity higher than 98%. Solvents such as methanol (MeOH), ethanol, cyclohexane (CHX), heptane (HP), and butyl acetate (BA) were purchased from PENTA (Prague, Czech Republic).
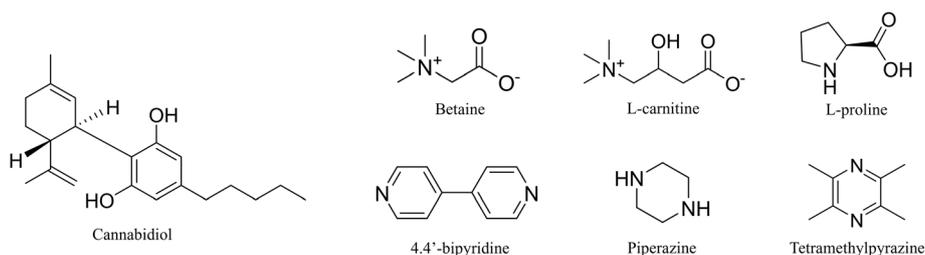

Fig. 1 Structures of cannabidiol and its coformers that create cocrystals.

2.2. Screening and cocrystal preparation

The screening of CBD cocrystals was performed in a 1:1 ratio for all initial experiments. For the screening experiments, we selected 28 coformers based on the type of their functional group (such as carboxylic, hydroxyl, alcohol), pK_α, molecular size, and hydrogen-bonding propensity using the Cambridge Structure Database (CSD). Some of the coformers used (*e.g.*, caffeine, L-carnitine, L-proline) can be found in the GRAS database. To consider all these possible properties, we also selected some coformers that are not pharmaceutically acceptable, such as 2,2′-bipyridine and 4,4′-bipyridine, but they can provide us further insight into the cocrystal formation and behaviour. This type of knowledge-based selection increases the probability of forming new cocrystals.[37] We also included five coformers, which are reported CBD cocrystals in the patent literature.[24,25]

2.2.1. Slurry experiments. CBD (approximately 20 mg) and the coformer were suspended in heptane or a mixture of heptane and ethanol (ratio 95:5) in 2 ml vials. The slurry experiments were performed for 7 days at 25 °C and 750 rpm in a thermomixer. The obtained material was filtered and dried.

2.2.2. Milling experiments. Grinding experiments were carried out with a Retsch MM400 mixer mill. Approximately 50 mg of CBD and an equimolar amount of the coformer were mixed in a 2 ml polypropylene milling jar with two 5 mm stainless steel balls. Subsequently, a liquid additive (MeOH or HP) was added in an amount of 5 μl into the plastic jars which were immediately closed to prevent evaporation of the liquid additive. The milling experiments were carried out at a frequency of 25 Hz for 20 minutes.

2.2.3. Single crystal preparation. The single crystal of CBD–BP was prepared by combining CBD and 4,4′-bipyridine in a 10:1 mixture of heptane and 1,4-dioxane, while CBD–PR was prepared in methanol. Both cocrystals were prepared by using CBD and the respective coformer in an equimolar ratio. These mixtures were heated to 35 °C to dissolve the powder and then left to cool down followed by slow evaporation until the single crystals were formed. The single crystals were consequently measured according to the conditions which are described below. The preparation of both single crystals did not present any challenges as opposed to the other forms. The crystal structure of the CBD–TMP cocrystal was not possible to be solved, because the single crystals were tiny needles with a very low refractive index. Nevertheless, we tried to employ XRPD to solve its crystal structure. However, all attempts failed because of the crystal structure's broad diffraction profile and complexity. We also tried to prepare single crystals of CBD–CR and CBD–PI by solvent evaporation or vapor diffusion, but all the experiments resulted in glassy oils. For this reason, we used XRPD to determine the cocrystal structure. However, we succeeded to solve only the crystal structure of CBD–CR.

2.3. Characterization

2.3.1. Powder X-ray diffraction (XRPD). The diffraction patterns were obtained for the raw powders and the prepared materials using a powder diffractometer X'Pert³ Powder (PANalytical, Holland) equipped with a Cu Kα anode (λ = 1.542 Å) with a tube voltage of 40 kV and a tube current of 30 mA. The samples were measured from 4 to 40° 2θ with a 0.026° 2θ step size and 56.87 s per step.

2.3.2. Single crystal and powder X-ray diffraction for the structure solution. The analysis of CBD–BP and CBD–PR was performed at 95 K using a SuperNova diffractometer with a micro-focus sealed tube, mirror-collimated Cu-Kα radiation (λ = 1.54184 Å), and a CCD detector Atlas S2. The data reduction and absorption correction were done with CrysAlisPro software.[38] The structures were solved by charge flipping methods using Superflip software and refined by full matrix least squares on squared value using Crystals and Jana2020 (ref. 39 and 40) software. MCE software was used for the visualization of residual electron density maps.[41] All H atoms were placed from the residual electron density map and the C–H bonds were constrained to ideal geometries. The single crystal sample of CBD–BP was twinned, and the structure was successfully solved from the main twin component. The structure of CBD–PR is slightly disordered, with one of the CBD side chains being in two positions with occupancies of 0.8 and 0.2.

The sample CBD–CR was ground and placed in a 0.5 mm borosilicate-glass capillary. Powder diffraction data were collected using the Debye–Scherrer transmission configuration on a powder diffractometer Smartlab of Rigaku (λCu, Kα1 = 1.54056 Å) that was equipped with a primary monochromator, focusing mirror, capillary holder and D/tex ultra 250 detector. The XRPD pattern was measured from 3° to 80° 2θ with a step size 0.01°. The overall measurement time was 20 h. The structures were deposited in the Cambridge Structural Database under numbers 2333022 (CBD–BP), 2333083 (CBD–PR) and 2333084 (CBD–CR). Details of the crystal structure solutions are in the ESI† in section S1.

2.3.3. Thermal analysis. Thermal properties were studied using differential scanning calorimetry (DSC 3+, Mettler Toledo, Switzerland) and thermogravimetric analysis (TGA). For DSC measurements, an aluminium pan was filled with 2 mg of sample. The aluminum pan was sealed and pierced to allow possible solvent vapour to escape and prevent an explosion. The investigation temperature range was from 20 °C to the specific degradation temperature of each sample, with a heating rate of 10 °C min⁻¹. In the TGA experiments, the pan was filled with approx. 2 mg of sample and heated from 30 °C to 300 °C with a heating rate of 5 °C min⁻¹. All measurements were carried out in an inert gas atmosphere.

2.3.4. Solution and solid-state nuclear magnetic resonance (NMR). Solution NMR was utilized to determine the stoichiometry and purity of the prepared materials. The samples were dissolved in d_6-DMSO and the ¹H NMR spectra were measured using an Avance III 500 MHz NMR spectrometer (Bruker, USA) equipped with a Prodigy probe and with a repetition delay of 10 s.

Solid-state NMR was used to confirm cocrystal creation and the purity of the obtained materials. The ¹³C NMR

spectra were measured using an Avance III 400 MHz NMR spectrometer (Bruker, USA) equipped with a 4 mm probe and with 13 kHz spinning.

2.4. Intrinsic dissolution rate (IDR)

2.4.1. Preparation and measurement of IDR samples. The IDR was measured using a Sirius inForm (Pion Inc., USA) connected to offline HPLC (high performance liquid chromatography) detection. The IDR discs with a diameter of 3 mm filled with *ca.* 20 mg of sample were compressed with a constant load of 100 kg, relaxed for one minute, and compressed again with approximately 100 kg for the second minute. The intrinsic dissolution rate was measured in 40 ml of 0.01 M hydrochloric acid buffer solution (pH = 2.0) with the addition of 0.5% Tween 20 at 100 rpm. The samples for HPLC analysis were taken every two minutes in an amount of 800 μl. After each sampling, the taken amount was immediately replaced with a fresh dissolution medium to maintain a constant volume. Each sample was measured in triplicate. The IDR was calculated using a linear fit of the 40 minutes of the measurement. The first six minutes were excluded from the analysis, because they represent the first dissolution of the free non-compressed powder from the disc surface created during preparation. After each measurement, the discs underwent XRPD analysis to confirm the crystal structure of all samples and refute any potential changes in polymorphism.

2.4.2. HPLC analysis. The HPLC analysis was performed using a Waters Alliance e2695 separation module (Agilent Technologies Inc., USA) with a high-pressure pump, an autosampler, a thermostat and a photodiode-array detector. A Waters XBridge C18 column (Waters Corporation, USA) with dimensions of 50 mm length and 4.6 mm internal diameter with a particle size of 3.5 μm was used for the analysis of the released API. The autosampler temperature was set to 25 °C, and the column heater was set at 40 °C during analysis. Ultrapure water with addition of formic acid (0.1%) and acetonitrile was used as components A and B, respectively, of the mobile phase for the separation. The gradient elution was set as follows: t (min)/% B: 0/30; 1.5/30; 6.5/80; 9/80; 9.5/30; 12/30 with the flow rate of the mobile phase being 0.8 ml min^{-1}. The injection was set to 50 μl for each sample. For evaluation of the released amount of API, the absorbance at 210 nm was used. The chromatographic data were evaluated using the software Empower™.

2.5. Stability study

2.5.1. Preparation of samples for stability tests. Samples for stability measurements were prepared by weighing *ca.* 50 mg of pure CBD and each multicomponent form into 2 ml dark glass vials. Then, the samples were put into dark stability chambers set to appropriate conditions. All powders were stored at 40 °C and 75% relative humidity (RH) for 25 days, at 60 °C and 40% or 75% RH for 13 days, and at 80 °C and 40% or 75% RH for 3 days. All the samples were

prepared in duplicate for each condition. After a specific time for each condition, the samples were taken from the chambers and analysed. The samples for UPLC (ultra performance liquid chromatography) measurement were diluted in methanol to a final concentration of 1 mg ml^{-1}.

2.5.2. UPLC purity analysis. The UPLC analysis was performed using a 1290 Infinity II LC system (Agilent Technologies Inc., USA) with a high-pressure pump, an autosampler, a thermostat and a diode array detector. An Acquity UPLC CSH Phenyl-Hexyl column (Waters Corporation, USA) with dimensions of 150 mm length and 2.1 mm internal diameter with a particle size of 1.7 μm was used for the purity analysis. The autosampler temperature was set to 5 °C, and the column heater was set at 20 °C during analysis. For the separation, ultrapure water and acetonitrile were used as components A and B, respectively, of the mobile phase. The gradient elution was set as follows: t (min)/% B: 0/50; 12/75; 14/100; 20/100; 20.5/50; 24/50. The flow rate of the mobile phase was 0.3 ml min^{-1}. The injection was set to 2 μl for each sample. The detection was performed using a UV/vis detector operated at a wavelength of 237 nm. The chromatographic data were evaluated using the software OpenLab CDS.

2.5.3. Statistical analysis. The data were processed by applying paired Student's significant test. The analysis focuses on calculation of p-values to determine the significance of the correlations between the obtained data. We used three different significance levels (α = 0.1, 0.05, 0.01) for data description. The data with significant difference $p < 0.1$ are marked with *, $p < 0.05$ with **, and $p < 0.01$ with ***, which is considered statistically significant.

2.5.4. Dynamic vapour sorption analysis (DVS). The DVS isotherms for all phases and pure CBD were measured using an SPS23-100n (ProUmid GmbH & Co. KG, Germany). The samples were exposed to a sorption cycle, and the relative humidity was gradually increased from 0% to 90% in steps of 10%. The weighing interval was 15 min. The minimum time per climate setting was 180 minutes, and the maximum was 30 hours, depending on the relative humidity level and the time required for the sample to reach equilibrium. The isotherms were measured at 25 °C.

2.5.5. Interaction energy calculations (and energy frameworks). Interaction energies and energy frameworks were calculated using the software CrystalExplorer17 version 17.5, revision f4e298a.[42] Molecular wavefunctions were obtained using the built-in Tonto utility at the "accurate" setting using the B3LYP/6-31G(d,p) level of theory. The pictures of the energy frameworks were created using the same software.

3. Results and discussion

3.1. Screening experiments

3.1.1. Slurry experiments. To initially confirm the formation of cocrystals obtained by slurry and milling experiments, the samples were analysed by XRPD. Four
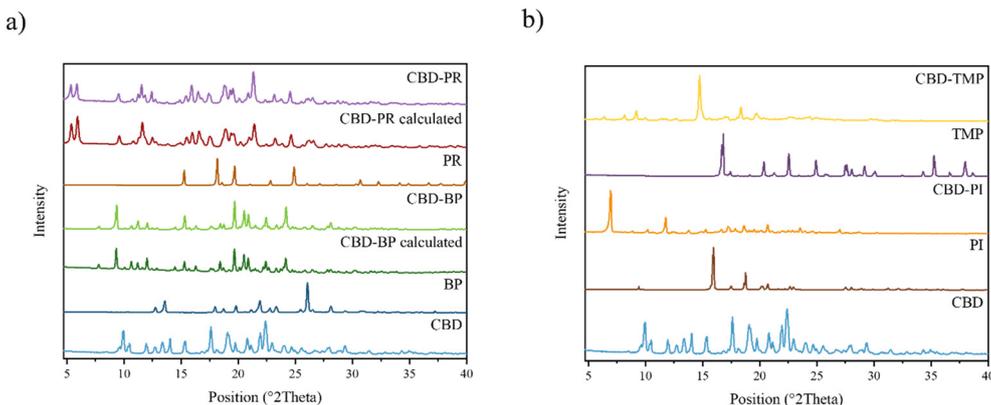
Fig. 2 a) Experimental and calculated XRPD patterns of CBD–BP and CBD–PR cocrystals prepared by the slurry method compared to their starting materials and b) experimental XRPD patterns of CBD–PI and CBD–TMP cocrystals compared to their starting materials.

cocrystals were prepared by the slurry method, namely CBD–BP, CBD–PI, CBD–PR, and CBD–TMP out of 29 tried coformers. The comparison of the XRPD patterns of the CBD cocrystals obtained by slurrying compared to the input materials and pure CBD is shown in Fig. 2. For those with solved crystal structures, simulated XRPD patterns are also shown to confirm their phase purity. All prepared phases exhibited X-ray diffractograms that were different from those of the starting materials.

3.1.2. Milling experiments. The same set of coformers was used for mechanochemical screening. As a liquid additive, we used MeOH, which is polar and may behave as a hydrogen donor or acceptor, and HP which is nonpolar. Liquid-assisted milling experiments may provide metastable forms of the same cocrystals or different cocrystals compared to the slurry method because more energy is applied to the system, and different interactions can be formed or broken.[43] Using the milling method, we successfully prepared the same cocrystals that were previously obtained with the slurry method, as described above.

The cocrystals with L-carnitine (CBD–CR) and betaine (CBD–BE) that were mentioned in the patent[24,25] were not within the positive results. To investigate if CBD–CR formation was possible under different conditions, we tried

milling with the addition of butyl acetate or cyclohexane as a liquid additive. In addition, we investigated different parameters such as the ratio of the substances, the amount of liquid additive and the period of milling. Although, in the patent literature, the cocrystal was prepared using cyclohexane, we were able to prepare it only using 5 µl of BA, a 1:1 ratio and a milling period of 100 min. The results of these experiments are shown in Fig. 3. The XRPD patterns of the solids obtained from all solvents, except BA, matched the XRPD pattern of the pure API. By using different ratios of CBD and CR, we observed changes in the intensity of the first peak near 6.92° 2θ. This peak is essential for the cocrystal, and it was getting less intense using a higher ratio of CR. We can also observe the excess of CR in all ratios except 1:1 in positions, *e.g.*, 18.88 and 22.08° 2θ. We also attempted various conditions, including different solvents and ratios, to prepare CBD–BE in its pure cocrystal form. However, the resulting material consistently showed the excess of CBD. Thus, we did not involve this cocrystal in further characterization. During milling, no polymorphic changes of CBD were observed.

The molar ratio of the prepared phases was further confirmed by ^{1}H NMR. It showed that the ratio of all prepared cocrystals was 1:1. The ssNMR was employed to
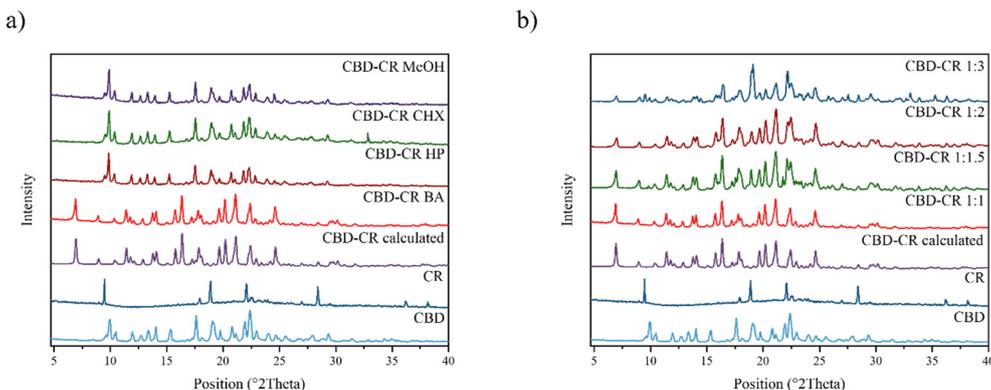

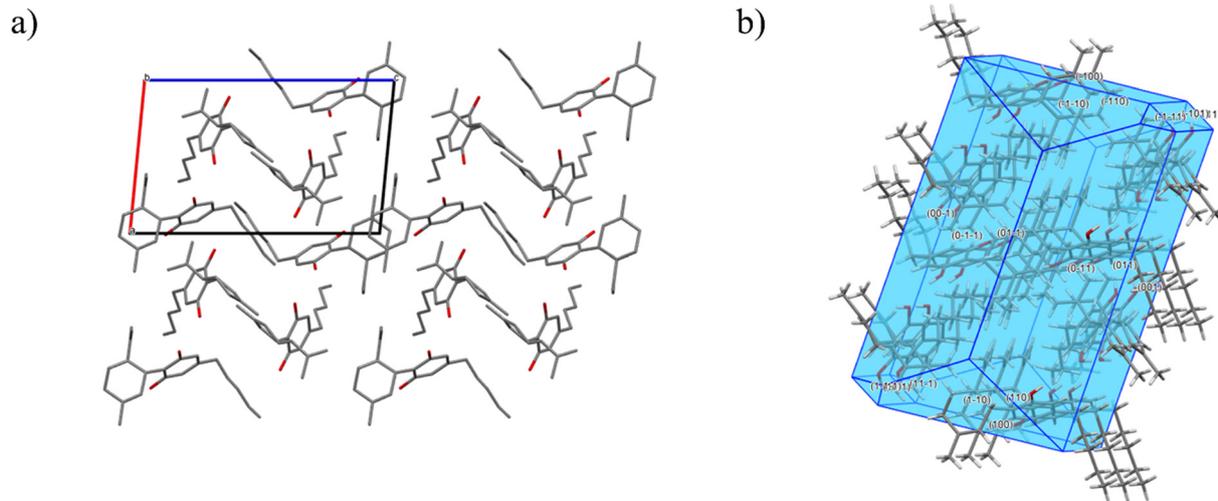**Fig. 3** XRPD patterns of CBD–CR a) using different solvents and b) using different ratios.

Fig. 4 Crystal structure of CBD: a) unit cell and b) predicted BFDH morphology.

provide further experimental evidence regarding the CBD cocrystals, confirming their formation by showing distinct changes in chemical shifts compared to the spectra of the input materials. The ssNMR spectra can be found in Fig. S2.†

3.2. Characterization

3.2.1. Crystal structures and morphology of the solid forms. To confirm the CBD multicomponent forms and get an insight into the crystal structure and its interactions, we tried to prepare single crystals for each form by using the methods of slow solvent evaporation and vapour diffusion. Crystal structures were successfully solved for the cocrystals CBD–BP, CBD–CR, and CBD–PR. The crystallographic data and details of refinement are presented in section S1.† For the solved structures, we also predicted the Bravais–Friedel–Donnay–Harker (BFDH) morphology using software Mercury 2.0 in order to describe which functional groups are exposed to the crystal surface.

3.2.1.1. CBD. The crystal structure of pure CBD has been known since 1977.[44,45] It crystallizes in the monoclinic system with the space group $P2_1$. The asymmetric unit (Fig. S3a†) consists of two molecules of CBD and the unit cell (Fig. 4a) is made in total by four molecules of CBD. The two molecules of CBD in the asymmetric unit are connected *via* oxygen atoms by a hydrogen bond (Fig. S3b†).

The calculated interaction energy among two CBD molecules is −60.6 kJ mol⁻¹ (Fig. S3c†). The BFDH predicted morphology of CBD (Fig. 4b) shows that on the crystal surface primarily exist the hydrophobic groups of CBD, which reduce the surface wettability.

3.2.1.2. CBD–BP. The CBD–BP cocrystal crystallizes in the monoclinic system with the space group $P2_1$. The asymmetric unit (Fig. S4a†) contains two molecules of CBD and two molecules of 4,4′-bipyridine, while in the unit cell (Fig. 5a), there are four molecules of each kind. The hydrogen bond pattern (Fig. S4b†) is quite simple and bonds CBD with two molecules of 4,4′-bipyridine. The molecules of CBD create a
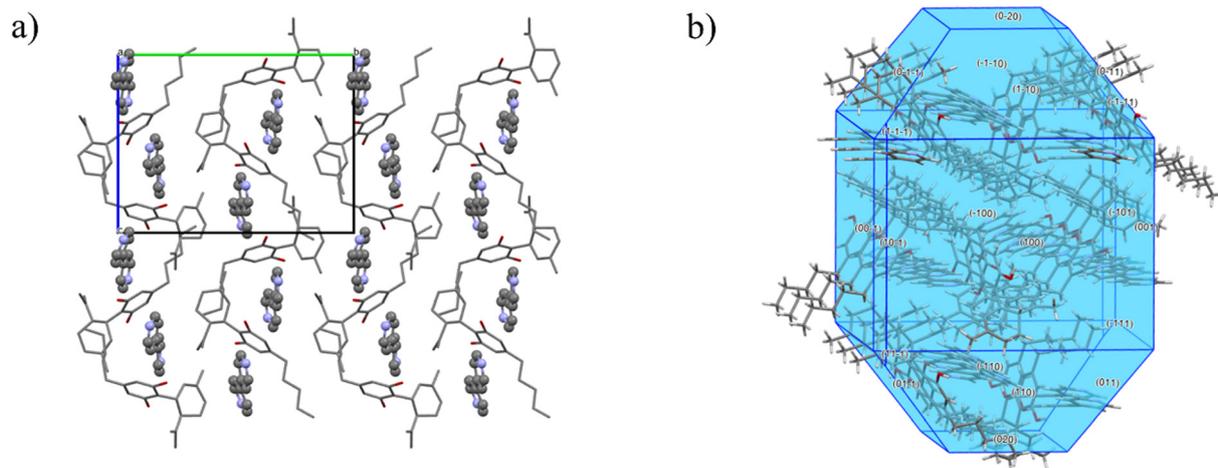

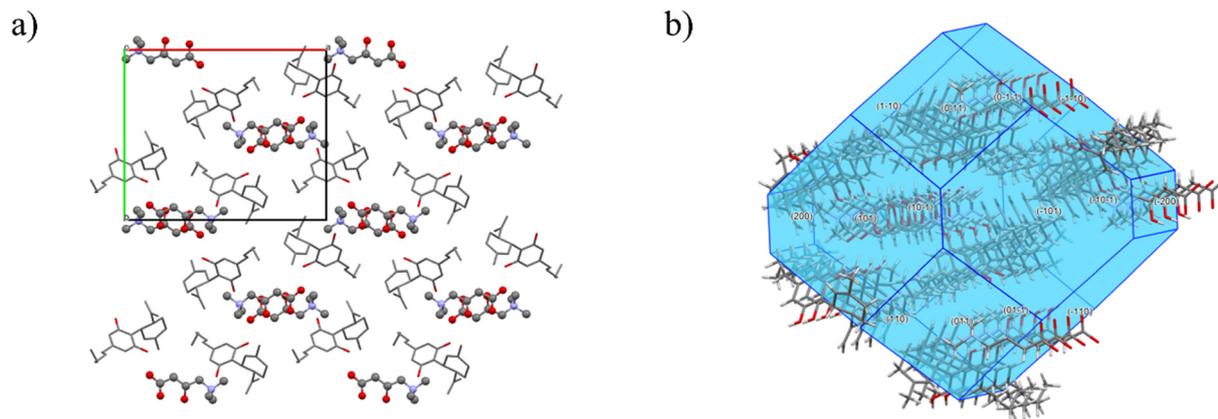Fig. 5 Crystal structure of CBD–BP: a) unit cell and b) predicted BFDH morphology.

a) b)

Fig. 6 Crystal structure of CBD–CR: a) unit cell and b) predicted BFDH morphology.

channel to host the molecules of 4,4′-bipyridine. 4,4′-Bipyridine molecules are arranged into layers and these layers are bonded by hydrogen bonding with CBD.

The strongest interaction energy is approximately −47.5 kJ mol^{-1} and it is between the molecules of CBD and bipyridine (Fig. S4c†). The interaction energy between the molecules of CBD is a little bit lower, around −37.7 kJ mol^{-1}. The predicted BFDH morphology (Fig. 5b) shows that CBD exhibits its hydrophobic groups (aliphatic chain) in majority on the crystal surface. On the crystal surface, the hydrophilic groups of CBD can also be found; however, they are placed on the smaller faces. Hence, the cocrystal would mostly exhibit hydrophobic behavior by itself.

3.2.1.3. CBD–CR. The cocrystal CBD–CR crystallizes in the orthorhombic system with the $P2_12_12_1$ space group. In the asymmetric unit (Fig. S5a†), there is one molecule of each CBD and L-carnitine. The unit cell (Fig. 6a) contains four molecules of each kind. The hydrogen bonding system (Fig. S5b†) is quite complex, and it involves bonding between CBD and L-carnitine and also within the molecule of L-carnitine between the carbonyl and hydroxyl groups. The molecules of L-carnitine are located in the channels, which are created by the CBD molecules.

The molecules of L-carnitine and CBD are connected with relatively weak interaction energies. The strongest of these interaction energies is approximately −23.8 kJ mol^{-1} (Fig. S5c†). The BFDH morphology (Fig. 6b) shows that mostly hydrophilic groups (carboxylic group of L-carnitine and hydroxy group of CBD) are exposed on the crystal surface of the cocrystal. This means that the cocrystal may easily interact with the atmospheric moisture, which may influence its physicochemical properties.

3.2.1.4. CBD–PR. The CBD–PR cocrystal has an orthorhombic symmetry with the space group $P22_12_1$. In its asymmetric unit (Fig. S6a†), it has two molecules of CBD and two molecules of L-proline, which are in the zwitterionic form. One molecule of CBD shows a disorder in the side aliphatic chain. The unit cell (Fig. 7a) consists of 8 molecules of each CBD and PR. There are several hydrogen bonds in the crystal structure (Fig. S6b†). The most significant are four H-bonds between the CBD and L-proline molecules that are arranged in a square. The H-bonding connects L-proline molecules together, by bonding NH and carbonyl groups, as well as connects the CBD molecule with L-proline through carbonyl and hydroxyl groups.

The strongest interaction energy (Fig. S6c†) can be found between two molecules of CBD (approximately −36.8 kJ mol^{-1}),
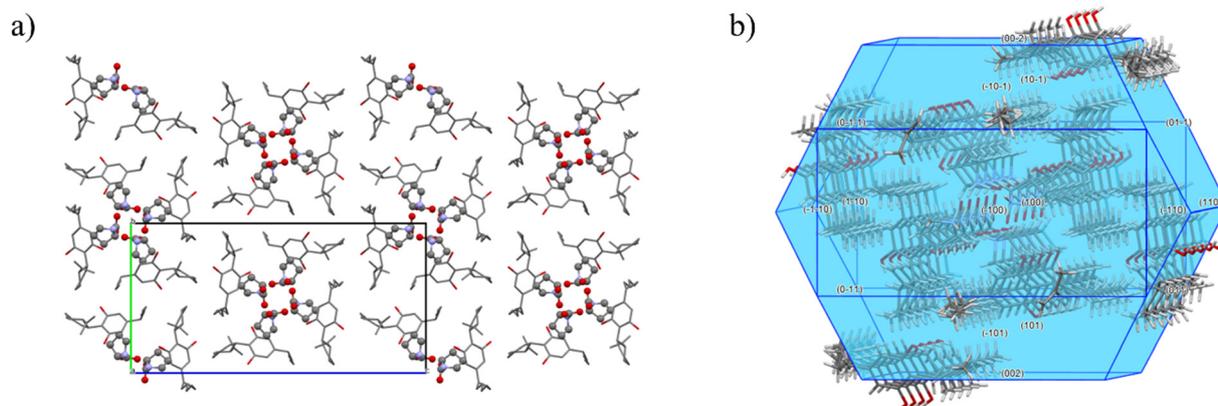
a) b)

Fig. 7 Crystal structure of CBD–PR: a) unit cell and b) predicted BFDH morphology.

while there are also interactions between the molecules of CBD and L-proline, but they are below 20 kJ mol^{-1} which is our cut off. The predicted BFDH morphology (Fig. 7b) shows both hydrophobic (aliphatic tail of CBD) and hydrophilic (hydroxy group of CBD) groups on the crystal surface of the cocrystal. However, the hydrophobic part shown on the surface is dominant.

3.3. Thermal analysis

Further characterization of the cocrystals in terms of their thermodynamic stability was provided by TGA and DSC analysis. The TGA and DSC results are shown in Fig. 8. From the TGA curves (Fig. 8a), a weight loss of approximately 34% for CBD–BP, 19% for CBD–PI and 27% for CBD–TMP is observed at temperatures near 180 °C, 160 °C and 100 °C, respectively. The weight loss is caused by the sublimation of the coformer in the cocrystal structure. However, as shown in Fig. S4,† the coformers completely sublimate at approximately 160 °C, 130 °C and 100 °C, respectively, when not part of a cocrystal. The higher sublimation temperature observed for the coformers in the cocrystals may result from interactions within the cocrystal structure, which probably require additional energy to overcome. For CBD–CR, a weight loss of 34% is also observed at 180 °C, which is attributed to the partial degradation of the coformer alone. The observed weight losses align with the calculated molar mass percentages of the coformers in the cocrystals. The DSC and TGA curves of the starting materials compared to the cocrystals can be found in section S4.† Only in the case of CBD–PR that we do not see any weight loss while heating because L-proline shows a higher thermal stability than the cocrystal itself.

From the DSC curves (Fig. 8b), we can observe that the pure CBD shows the melting onset at 62 °C and a peak at 67 °C. In contrast, all new phases show higher melting points; CBD–PI melts at 85 °C (T_{onset} = 77 °C), CBD–TMP at 93 °C (T_{onset} = 90 °C), CBD–BP at 135 °C (T_{onset} = 132 °C), CBD–PR at 149 °C (T_{onset} = 140 °C) and CBD–CR at 153 °C (T_{onset} = 147 °C). The last three mentioned cocrystals showed at least a double increase in the melting point compared to the pure

CBD. However, for the samples CBD–BP, CBD–PI, and CBD–TMP, the melting event is accompanied by the decomposition of the coformer, which is shown in Fig. 8a.

The higher melting point of the multicomponent solid forms is often believed to indicate higher thermal stability of the cocrystals. But when comparing the melting temperature of the solid forms with their interaction energies, we can see that a higher melting point does not always indicate higher interaction energies of the crystal. For example, for CBD–CR which has a melting point of 153 °C, we observed that it has a relatively low energy between its molecules (-23.8 kJ mol^{-1}), which is the lowest compared to the other cocrystals. In addition, CBD–BP with the third highest melting point (135 °C) still shows a lower interaction energy between the molecules (-47.5 kJ mol^{-1}) compared to pure CBD (-60.6 kJ mol^{-1}), even though the interaction energy between the molecules of CBD–BP is the highest among the cocrystals. This suggests that the stability of cocrystals in general is a more complicated property than we would expect, and it depends on many parameters such as the crystalline lattice arrangement, symmetry, interaction energies, hygroscopicity of the cocrystals, etc.[46]

3.4. Dynamic vapour sorption

We performed first the DVS analysis (Fig. 9) to get further insight into the stability behaviour of the multicomponent solid forms when exposed to humidity. The stability of the cocrystals against atmospheric moisture is believed to be also connected to the crystal morphology.[47]

The pure CBD powder exhibited a low absorption of water even for a high relative humidity, which is in accordance with its natural hydrophobicity.[1,14] The same hydrophobic behaviour as that of pure CBD was observed for cocrystal CBD–BP. The CBD–PR sample becomes slightly hygroscopic when exposed to relative humidity levels exceeding 80%. The DVS results are in accordance with the predicted BFDH morphologies (section 2.3.2) of these cocrystals. Both structures exhibit a higher number of hydrophobic groups on their crystal surfaces, which reduces their interaction with
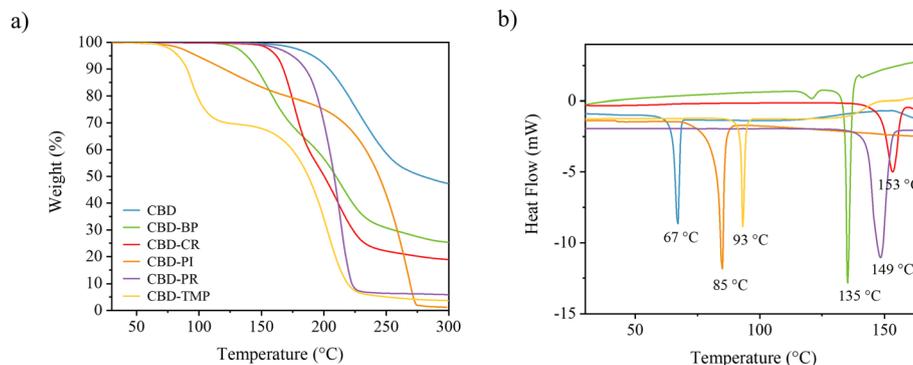

Fig. 8 a) TGA thermograms and b) DSC thermograms of CBD and the cocrystals CBD–BP, CBD–CR, CBD–PI, CBD–PR, and CBD–TMP.
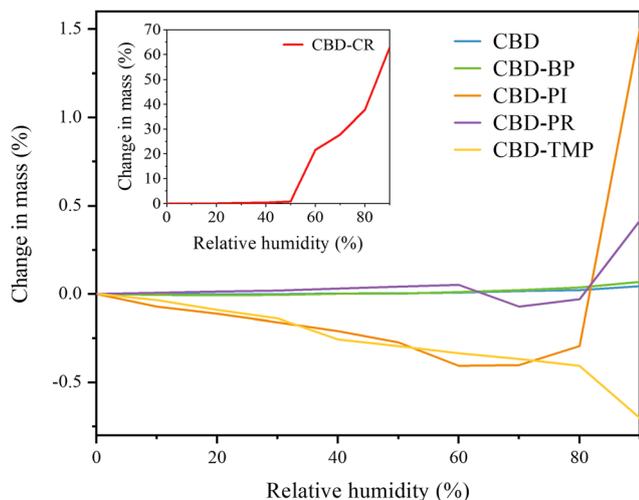
Fig. 9 The DVS curves of CBD and its cocrystals.

atmospheric moisture. On the other hand, CBD–TMP shows only a decrease of the mass, which is connected to the tendency of tetramethylpyrazine to sublimate.[48] TMP by itself absorbs water rapidly for RH $\geq$ 50% (ref. 48); however, the formation of the cocrystal probably protects TMP to remain not hydrated even for high RH. The CBD–PI cocrystal shows also a decrease of the mass up to 80% RH, which is connected to the sublimation of PI, which occurs even under standard conditions.[49] The higher hygroscopic tendency of piperazine[50] probably influences the behaviour of the cocrystal for higher ($\geq$80% RH) humidity, when it becomes slightly hygroscopic. Contrary to all multicomponent forms and pure CBD, CBD–CR exhibits a high-water absorption for RH $\geq$ 50%; the weight of the sample reached *ca.* 63% for 90% RH. This high water absorption may be connected to the high hygroscopic tendency of ʟ-carnitine, which was also reported as a problem for tablet manufacturing due to the adhesion of tablets to punches.[51] Furthermore, the BFDH morphology prediction shows mostly hydrophilic groups on the crystal surface, which probably interact easily with the atmospheric moisture.

3.5. Intrinsic dissolution rate

The IDR measurements were performed for pure CBD and its cocrystals. The dissolution study was carried out in hydrochloride acid buffer (pH = 2) to mimic the environment of the stomach. The results are shown in section S5,† along with the exact IDR values and the dissolution rate profiles for all cocrystals and pure CBD. All the cocrystals showed lower IDR values than pure CBD (13.05 $\pm$ 0.32 μg min^{-1} cm^{-2}).

To gain further insight into the dissolution mechanism, we performed XRPD analysis of the disks after dissolution (Fig. S11†). In all cases, we observed peaks of cocrystals together with the pure CBD suggesting partial transformation of cocrystals after exposure to the water environment. The observed transformation of the cocrystals might be connected

to weak interaction energies between the molecules of CBD and coformers and the hydrophilic nature of the coformers, which contain polar functional groups. The combination of these factors suggests that the cocrystals are unstable in an aqueous environment, leading to their dissociation into the coformer and CBD. Thus, CBD becomes available for dissolution only after this dissociation process occurs. Given that cocrystal decomposition follows a kinetic pathway, this phenomenon likely contributes to the slightly slower dissolution rates observed for the cocrystals (Fig. S9†). This hypothesis is further supported by the behaviour of CBD–CR, where its more hydrophilic surface coupled with a low interaction energy (-23.8 kJ mol^{-1}) allows easier contact of the cocrystal with water and faster decomposition, therefore resulting in a higher IDR compared to the other cocrystals.

3.6. Stability and degradation studies

The stability and degradation studies were performed to describe the behaviour of the multicomponent solid forms compared to the pure CBD under accelerated storage conditions. We analysed the amount of CBD in the samples and checked the visual changes (colour and state of the powder) and the crystalline state after removing the samples from stability chambers. All the samples before the accelerated stress study were white powders, except for CBD–PI which was originally brownish. The results are shown in Fig. 10.

As can be seen, pure CBD showed a considerable difference in the CBD amount in each case except for storage at 40 °C/75% RH and 60 °C/75% RH where it remained stable, as confirmed by both UPLC and XRPD analyses (Fig. S12a†). However, the sample stored at 60 °C/40% RH and at 80 °C, showed a higher decrease in purity of CBD, and furthermore the samples changed into a jelly-like state with a brownish colour, which is caused by the fact that the storage conditions are close to or even exceed the melting point of CBD.

For the CBD–BP cocrystal, no significant decrease of CBD was observed, and it remained stable the whole time of the experiment under different conditions. Furthermore, the stability of the sample in each condition was confirmed using XRPD (Fig. S12b†); all the samples remained in the powder unchanged state.

Storing CBD–CR at 40 °C/75% RH for 25 days did not cause any decrease in the amount of CBD. However, XRPD analysis confirmed a change in the solid state of the sample (Fig. S12c†). The XRPD pattern shows almost the same peaks as those of pure CBD, but we can also identify peaks belonging to ʟ-carnitine (*e.g.*, 9.46, 17.94, 18.89° 2θ). This observation suggests that after storing, the cocrystal starts to become disintegrated to the initial compounds. Under the 60 °C/40% RH conditions, only a slight decrease in the CBD amount was observed, and the cocrystal pattern remained preserved, as shown by the XRPD results. Storing CBD–CR under the remaining conditions led to a significant decrease in the CBD amount, and the samples also deliquesced. These results,
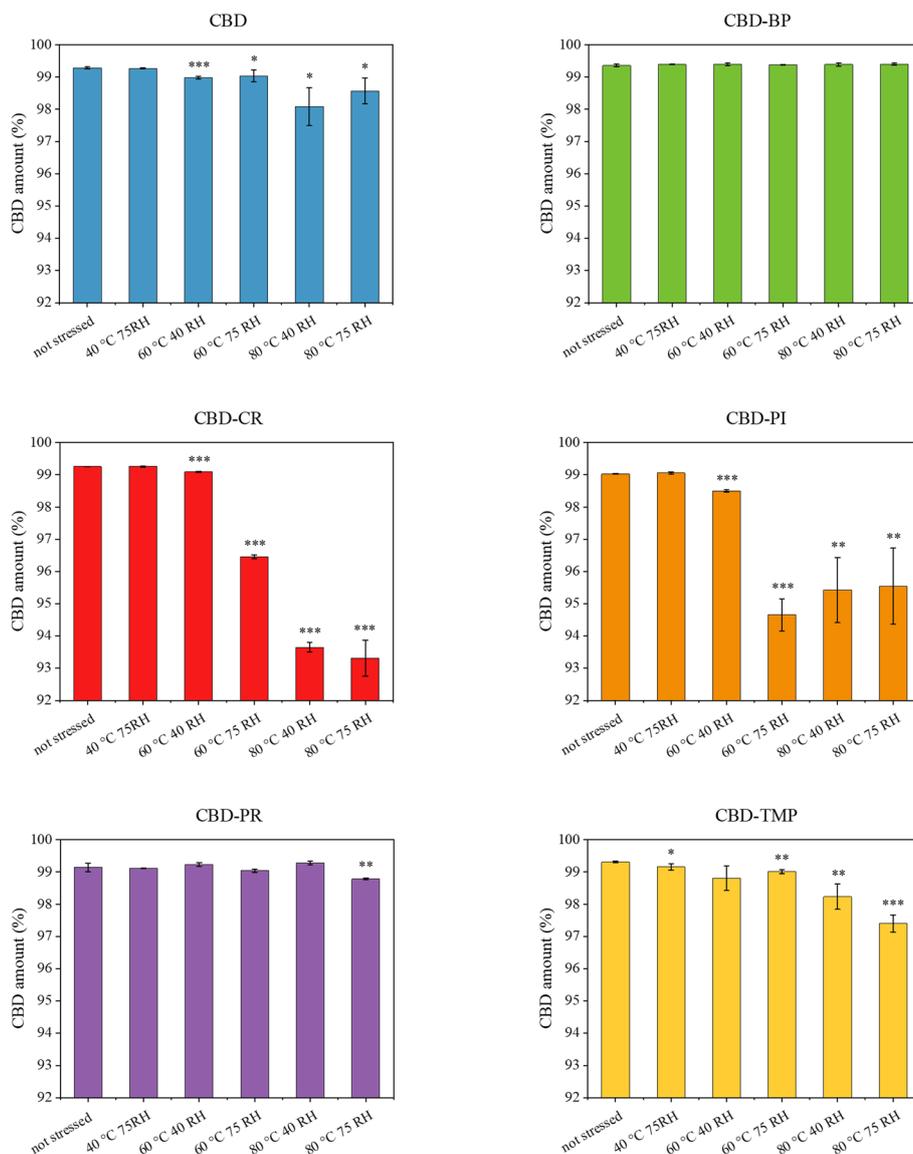
Fig. 10 The CBD amount in the not stressed cocrystals and pure CBD compared to the CBD amount for the cocrystals and pure CBD after accelerated stress conditions.

combined with the DVS data, show evidence that L-carnitine exhibits high water absorption. It can be assumed that the stability of CBD–CR is also highly dependent on the applied relative humidity.

The CBD amount in the sample CBD–PI remained stable while stored at 40 °C/75% RH, and furthermore the solid state remained stable according to XRPD (Fig. S12d†). The rest of the used conditions led to a statistically significant decrease in the amount of CBD. The samples stored at 60 °C and 80 °C changed into a jelly-like state after removing them from the chambers. This may be caused by the fact that the storage temperature is close to its melting point.

When samples of CBD–PR were stored under all conditions, the CBD amount and the crystalline state remained stable, except for the sample stored at 80 °C/75% RH. In that case, the colour of the sample changed into a darker beige colour, which may be connected to the water

absorption in the environment with extreme conditions. Nevertheless, the XRPD analysis (Fig. S12e†) confirmed the initial cocrystal state.

CBD–TMP showed a decrease in the amount of CBD while stored under different conditions. The sample stored at 60 °C/40% RH changed its colour to red; however, the cocrystal formation was still preserved, which was confirmed by XRPD (Fig. S12f†). When storing the sample at 60 °C/75% RH, the XRPD analysis confirmed a change in the solid state. The XRPD pattern showed new peaks, *e.g.*, at 9.65, 10.14, and 15.02° 2θ corresponding to the pure CBD; however, there are still some peaks preserved corresponding to the cocrystal formation (*e.g.*, 8.95, 14.50, 18.10° 2θ). Therefore, we can expect that CBD–TMP is partially disintegrated into the initial compounds, but part of the cocrystal is still preserved. Both samples stored at 80 °C transformed into a jelly-like state, with a brown colour.

Overall, regarding the stability of multicomponent forms, the cocrystals with 4,4′-bipyridine and L-proline showed higher stability than the rest of the solid forms. Furthermore, they remained in a powder state throughout the entire storage period. We did not observe any melting or deliquescence, or water sorption of the powder. The high stability may be caused by the fact that in the BFDH morphology prediction, the crystal shows mostly hydrophobic parts on the surface, which probably protect the cocrystal from interaction with the atmospheric moisture that accelerates its disintegration. For the remaining cocrystals, we expect that humidity primarily influences their stability, rather than heat, because we observed their tendency to deliquesce even under conditions below their corresponding melting point. In the case of CBD–CR, the stability is mainly influenced by its crystal morphology, which exhibits mostly hydrophilic groups on the crystal surface. These groups may interact with the atmospheric humidity and probably lead to faster degradation of the cocrystal, although the cocrystal shows the highest melting point (153 °C). Furthermore, the calculation of interaction energies for the available crystal structures confirmed our observation, *e.g.*, in the case of CBD–CR, we obtained the lowest interaction energy (-23.8 kJ mol^{-1}) compared to the cocrystals with 4,4′-bipyridine (-47.5 kJ mol^{-1}) or L-proline (-36.8 kJ mol^{-1}), resulting in faster disintegration of the cocrystal. Apart from the already mentioned reasons, there are other ones that might accelerate and lower the stability of the cocrystal, such as higher surface area of the crystal or appearance of pores in the structure.

Regarding the degradation of the cocrystals, we could observe the same phenomenon as for the stability behaviour of the cocrystals. This means that the new solid forms with 4,4′-bipyridine and L-proline are protected from degradation by their high stability. On the other hand, the rest of the cocrystals show faster degradation, because of the lower stability of the cocrystals. Hence, we assume, according to the performed analyses, that the cocrystals are firstly disintegrated and consequently degraded by the applied humidity and heat.

4. Conclusion

In this study, we explored the synthesis and characterization of five CBD cocrystals, with the aim of investigating their physicochemical properties. Thermal analysis revealed that all cocrystals demonstrated higher melting points compared to the pure CBD. It was found that the intrinsic dissolution rate of the cocrystals was slightly lower in all cases compared to the free CBD. This behaviour is probably due to their instability in an aqueous solution and their rapid dissociation, caused by low interaction energies between the CBD and coformer in combination with the hydrophilic nature of the coformers. To investigate further the stability of the cocrystals, we performed stability studies of all cocrystals and pure CBD under different humidity and temperature conditions. Among the tested cocrystals CBD–4,4′-bipyridine,

which did not exhibit the highest melting point, demonstrated the highest stability, showing no significant degradation under stress conditions. However, its potential in pharmaceutical applications is limited because 4,4′-bipyridine is not considered a pharmaceutically acceptable compound. CBD–L-proline also exhibited notable stability, likely due to its hydrophobic crystal surface and strong molecular interactions within the cocrystal. Our results emphasize that the melting point is not the sole determining factor for the stability of the cocrystals. It is important to consider also other factors, such as interaction energies of the molecules, surface morphology and hygroscopicity of the crystals. The demonstrated stability improvement in the cocrystal CBD–L-proline suggests its potential for further development as a solid-state form in pharmaceutical applications. Future research could explore optimization of the processing conditions to obtain this cocrystal in larger quantities. Additionally, *in vivo* studies could be conducted to reveal the therapeutic efficacy.

Data availability

Additional data are provided in the ESI† file. Crystallographic data for 2333022 (CBD–BP), 2333083 (CBD–PR) and 2333084 (CBD–CR) have been deposited at the Cambridge Structural Database.

Author contributions

Adéla Koryťáková – conceptualization, methodology, investigation, writing – original draft. Argyro Chatziadi – conceptualization, methodology, investigation, writing – review & editing. Jan Rohlíček – methodology, investigation, writing – review & editing. Eliška Zmeškalová – methodology, investigation, writing – review & editing. Josef Beránek – conceptualization, methodology, supervision, writing – review & editing. Miroslav Šoóš – conceptualization, methodology, supervision, writing – review & editing, funding acquisition.

Conflicts of interest

There are no conflicts to declare.

Acknowledgements

References

1 L. Grifoni, G. Vanti, R. Donato, C. Sacco and A. R. Bilia, *Molecules*, 2022, **27**, 6070.

2   M. M. Radwan, S. Chandra, S. Gul and M. A. ElSohly, *Molecules*, 2021, **26**, 2774.

3   E. M. Williamson and F. J. Evans, *Drugs*, 2000, **60**, 1303–1314.

4   N. Peyravian, S. Deo, S. Daunert and J. J. Jimenez, *ImmunoTargets Ther.*, 2020, 131–140, DOI: **10.2147/ITT.S263690**.

5   B. Stella, F. Baratta, C. Della Pepa, S. Arpicco, D. Gastaldi and F. Dosio, *Drugs*, 2021, **81**, 1513–1557.

6   A. Fraguas-Sanchez, A. Fernández-Carballido, C. Martin-Sabroso and A. Torres-Suárez, *J. Chromatogr., B*, 2020, **1150**, 122188.

7   Epidyolex, **https://www.ema.europa.eu/en/medicines/human/EPAR/epidyolex**, (accessed 02.01.2024).

8   Sativex, **https://www.ema.europa.eu/en/medicines/human/paediatric-investigation-plans/emea-000181-pip02-13-m01**, (accessed 02.01.2024).

9   K. Knaub, T. Sartorius, T. Dharsono, R. Wacker, M. Wilhelm and C. Schön, *Molecules*, 2019, **24**, 2967.

10 S. A. Millar, R. F. Maguire, A. S. Yates and S. E. O'Sullivan, *Pharmaceuticals*, 2020, **13**, 219.

11 K. Hatziagapiou, K. Bethanis, E. Koniari, E. Christoforides, O. Nikola, A. Andreou, A. Mantzou, G. P. Chrousos, C. Kanaka-Gantenbein and G. I. Lambrou, *Pharmaceutics*, 2022, **14**, 706.

12 G. P. Andrews, *Philos. Trans. R. Soc., A*, 2007, **365**, 2935–2949.

13 Z. B. Shariff, D. T. Dahmash, D. J. Kirby, S. Missaghi, A. Rajabi-Siahboomi and I. D. Maidment, *J. Am. Med. Dir. Assoc.*, 2020, **21**, 1015–1023.

14 S. A. Millar, N. L. Stone, A. S. Yates and S. E. O'Sullivan, *Front. Pharmacol.*, 2018, **9**, 1365.

15 K. Mozaffari, S. Willette, B. F. Lucker, S. E. Kovar, F. O. Holguin and I. Guzman, *Molecules*, 2021, **26**, 3573.

16 P. Guruprasad Reddy, A. Bar-Hai, A. Hoffman, S. Marc Feldmann and A. J. Domb, *Bioorg. Chem.*, 2023, **141**, 106914.

17 O. Jennotte, N. Koch, A. Lechanteur and B. Evrard, *J. Drug Delivery Sci. Technol.*, 2022, **71**, 103372.

18 N. Koch, O. Jennotte, Y. Gasparrini, F. Vandenbroucke, A. Lechanteur and B. Evrard, *Int. J. Pharm.*, 2020, **589**, 119812.

19 H. E. Straker, L. McMillan, L. Mardiana, G. R. Hebberd, E. Watson, P. G. Waddell, M. R. Probert and M. J. Hall, *CrystEngComm*, 2023, **25**, 2479–2484.

20 N. Schultheiss and A. Newman, *Cryst. Growth Des.*, 2009, **9**, 2950–2967.

21 M. Guo, X. Sun, J. Chen and T. Cai, *Acta Pharm. Sin. B*, 2021, **11**, 2537–2564.

22 N. Qiao, M. Li, W. Schlindwein, N. Malek, A. Davies and G. Trappitt, *Int. J. Pharm.*, 2011, **419**, 1–11.

23 N. Shan and M. J. Zaworotko, *Drug Discovery Today*, 2008, **13**, 440–446.

24 Artelo Biosciences, Inc., US10604467B2, 2020.

25 S. L. Enantia, WO2019030158A1, 2019.

26 B. K. Kalita, D. Pathak, H. Sharma and B. Sarma, *Stud. Nat. Prod. Chem.*, 2023, **78**, 323–364.

27 Proprietary CBD:TMP Cocrystal for Anxiety & Depression, **https://artelobio.com/pipeline/art12-11/**, (accessed 18.07.2024).

28 R. Mechoulam and L. R. Hanuš, *Chem. Phys. Lipids*, 2002, **121**, 35–43.

29 J. Yangsud, S. Santasanasuwan, P. Ahkkarachinoreh, A. Maha, F. Madaka, J. Suksaeree, T. Songsak, A. Vutthipong and C. Monton, *Adv. Tradit. Med.*, 2021, **21**, 475–484.

30 W. Jaidee, I. Siridechakorn, S. Nessopa, V. Wisuitiprot, N. Chaiwangrach, K. Ingkaninan and N. Waranuch, *Cannabis Cannabinoid Res.*, 2021, **7**, 537–547.

31 C. Franco, S. Protti, A. Porta, F. Pollastro, A. Profumo, B. Mannucci and D. Merli, *Results Chem.*, 2022, **4**, 100465.

32 H. Zheng, B. Chen and J. Rao, *Food Funct.*, 2022, **13**, 4502–4512.

33 V. N. Tran, O. Strnad, J. Šuman, T. Veverková, A. Sukupová, P. Cejnar, R. Hynek, O. Kronusová, J. Šach, P. Kaštánek, T. Ruml and J. Viktorová, *Int. J. Pharm.*, 2023, **643**, 123202.

34 K. B. Scheidweiler, M. Andersson, M. J. Swortwood, C. Sempio and M. A. Huestis, *Drug Test. Anal.*, 2017, **9**, 143–147.

35 E. Kosović, D. Sýkora and M. Kuchař, *Pharmaceutics*, 2021, **13**, 412.

36 O. González-González, I. O. Ramirez, B. I. Ramirez, P. O'Connell, M. P. Ballesteros, J. J. Torrado and D. R. Serrano, *Pharmaceutics*, 2022, **14**, 2324.

37 M. Singh, H. Barua, V. G. S. S. Jyothi, M. R. Dhondale, A. G. Nambiar, A. K. Agrawal, P. Kumar, N. R. Shastri and D. Kumar, *Pharmaceutics*, 2023, **15**, 1161.

38 Agilent, *CrysAlis PRO*, Agilent Technologies Ltd, Yarnton, Oxfordshire, England, 2014.

39 V. Petříček, L. Palatinus, J. Plášil and M. Dušek, *Z. Kristallogr. – Cryst. Mater.*, 2023, **238**, 271–282.

40 L. Palatinus and G. Chapuis, *J. Appl. Crystallogr.*, 2007, **40**, 786–790.

41 J. Rohlíček and M. Hušák, *J. Appl. Crystallogr.*, 2007, **40**, 600–601.

42 C. F. Mackenzie, P. R. Spackman, D. Jayatilaka and M. A. Spackman, *IUCrJ*, 2017, **4**, 575–587.

43 A. Chatziadi, E. Skořepová, J. Rohlíček, M. Dušek, L. Ridvan and M. Šóóš, *Cryst. Growth Des.*, 2020, **20**, 139–147.

44 P. G. Jones, L. Falvello, O. Kennard, G. Sheldrick and R. Mechoulam, *Acta Crystallogr., Sect. B: Struct. Crystallogr. Cryst. Chem.*, 1977, **33**, 3211–3214.

45 T. Ottersen, E. Rosenqvist, C. Turner and F. El-Feraly, *Acta Chem. Scand., Ser. B*, 1977, **31**, 807–812.

46 A. Chatziadi, E. Skorepova, J. Jirat, J. Rohlíček and M. Šóóš, *Cryst. Growth Des.*, 2022, **22**, 3395–3404.

47 R. Thakuria, M. Arhangelskis, M. D. Eddleston, E. H. H. Chow, K. K. Sarmah, B. J. Aldous, J. F. Krzyzaniak and W. Jones, *Org. Process Res. Dev.*, 2019, **23**, 845–851.

48 Y. Xie, L. Gong, Y. Tao, B. Zhang, L. Zhang, S. Yang, D. Yang, Y. Lu and G. Du, *Molecules*, 2024, **29**, 2208.

49 L. Zaharani, M. R. Johan and N. G. Khaligh, *J. Therm. Anal. Calorim.*, 2022, **147**, 14183–14193.

50 X. Wang, S. Xu, L. Jia, Y. Yang, Y. Liu, J. Gong and S. Wu, *CrystEngComm*, 2019, **21**, 5284–5291.

51 A. A. Badawi, M. M. Hegazy, D. Louis and M. A. Eldegwy, *Acta Pharm.*, 2017, **67**, 511–525.